MASSACHUSETTS INSTITUTE OF TECHNOLOGY
LINCOLN LABORATORY

FLASHLIGHT RADAR: A THREE-DIMENSIONAL IMAGING RADAR

D.J. BLEJER
R.L. FERRANTI
R.M. BARNES
W.W. IRVING
S.M. VERBOUT
Group 47

PROJECT REPORT TT-74

10 AUGUST 1989

LEXINGTON MASSACHUSETTS

Abstract

In support of several programs at Lincoln Laboratory, a small focused-beam polarimetric, millimeter-wave radar scatterometer (an instrument for measuring radar cross section) has been developed. An overview of the design of this "Flashlight Radar" is presented. Theoretical and empirical studies of antenna performance are discussed. The backscatter theory relating to the characteristics of the Flashlight Radar as a scatterometer is presented, and experimental RCS measurements are compared with theoretical predictions. The data processing steps (polarimetric calibration and compensation, signal processing, and image formation) are described. We show the results of two representative experiments using the Flashlight Radar. The first is a measurement of dihedral and trihedral reflectors with and without radar camouflage. The second is a raster scan of a truck tire, highlighting the radar's fine resolution and its ability to collect three-dimensional data.

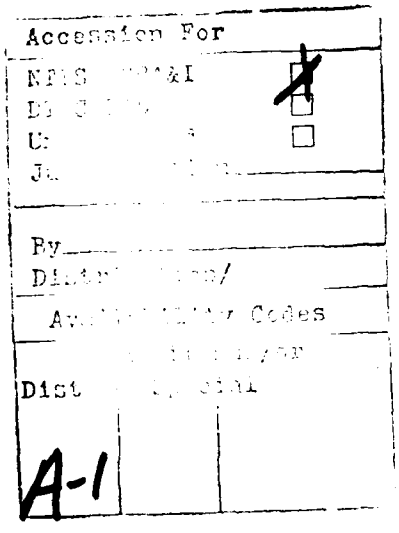

Contents

List of Figures

1 Introduction

The Flashlight Radar is a short-range, high-resolution, fully polarimetric FM−CW instrumentation radar intended for detailed scattering measurements of various targets. It was designed to fulfill three basic purposes. First, the Flashlight Radar supports Lincoln Laboratory's millimeter-wave, airborne synthetic aperture radar (SAR); the Flashlight Radar can be used in the field to investigate highly reflective target areas identified in the SAR images. The radar also supports our target modeling efforts, yielding detailed, two- and three-dimensional polarimetric images of both simple and complicated targets. Finally, the Flashlight Radar is used for a variety of other measurements, such as determining the scattering properties of materials and natural clutter.

The Flashlight Radar can collect data in one, two, or three dimensions. Its focused, horn-lens antenna yields a 4.6 inch diameter spot size at a distance of 10 ft. Fine range-resolution (six inches) results from the 1-GHz swept bandwidth. The radar operates at a center frequency of 35 GHz.

The instrument collects fully polarimetric data in the linear (horizontal and vertical) basis. This data can then be processed to produce images in any desired format, for example, linear or circular basis. They can be presented in one, two, or three dimensions. Also, the collected data can be processed to simulate larger beamwidths or coarser range resolution. Thus, for example, the Flashlight Radar might collect three-dimensional data from a target, but then process it to produce a two-dimensional lower-resolution image which simulates a synthetic aperture radar.

Section 2 of this report reviews the basics of FM−CW radar. Section 3 provides an overview of the design of the Flashlight Radar. In section 4, theoretical and experimental studies of antenna performance are discussed. The backscatter theory relating to the performance of the radar as a scatterometer (an instrument for measuring radar cross section) is presented in Section 5, and experimental RCS measurements are compared with theoretical predictions. Section 6 discusses the data processing steps: polarimetric calibration and compensation, signal processing to compensate for hardware imperfections, and image formation. Section 7 presents the results of two experiments using the Flashlight Radar. Section 8 describes other current and future applications of the instrument.

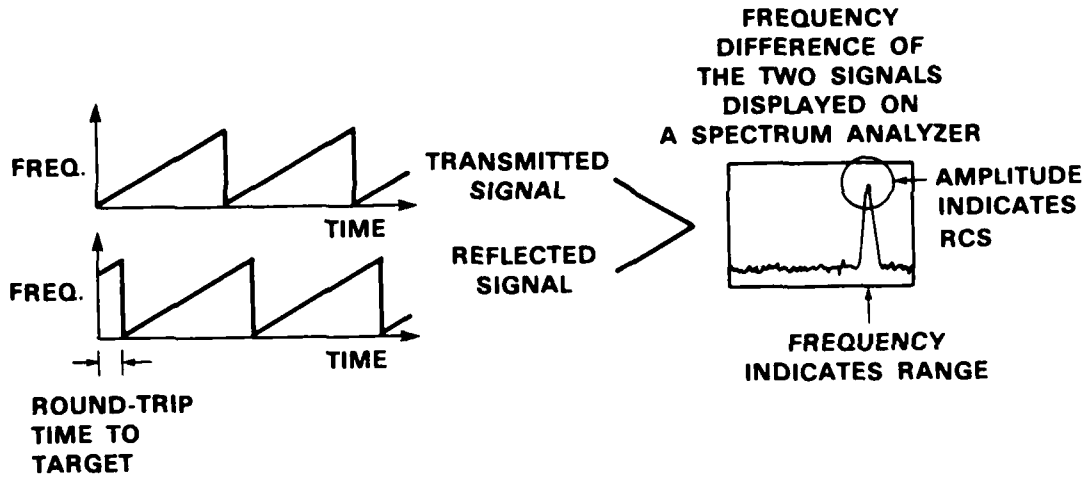

Figure 1: FM−CW radar operation.

2 FM−CW Radar Basics

The basic principle of FM−CW radar operation is illustrated in Figure 1. A constant-amplitude signal with a linearly increasing frequency is transmitted, and a distant point-target reflects a time-delayed version of the signal back to the radar. The original and reflected signals are processed to produce a difference signal with amplitude directly proportional to target radar cross section, and frequency directly proportional to target range. This signal is also coherent; that is, its phase tracks the two-way rf phase distance to the target. Because the system is linear, the signature of a complex target (i.e., a target composed of a number of point scatterers) will equal the vector sum of the signatures of the point scatterers.

Thus, when the Flashlight Radar illuminates a complex target, the raw output signal is a sum of sinusoids (a "phase history"). The Fourier transform of the phase history is a range profile. The horizontal position of a spike in a range profile corresponds to the range of the scatterer that produced it, while the amplitude of the spike is proportional to the radar cross section of the scatterer. As with any radar, the spike width (the range resolution) is determined by the swept-frequency bandwidth. Since the Flashlight Radar is a real-aperture system, the cross-range resolution is determined by the antenna beamwidth and the distance to the target.

3 Radar System Design

The Flashlight Radar was inspired by the "Sourcescat" FM−CW radar scatterometer built by R.K. Moore and others [1]. We scaled their 10 GHz design to 35 GHz, and also made it coherent and fully polarimetric. To maintain polarization purity, our design uses a focused horn-lens antenna instead of their offset-fed parabolic reflector. In addition, all of the Flashlight Radar data collection and processing is performed digitally.

Figure 2 is a detailed block diagram of the instrument. To maximize the isolation between the transmit oscillator and the receive mixers, the transmit/receive system is implemented with triple-junction circulators. In addition, isolators and attenuators reduce internal reflections. These precautions ensure a flat rf frequency response over the swept bandwidth. The swept-frequency source is a YIG-tuned GaAs Gunn oscillator, chosen because of its inherent linearity and low phase noise. A list of important Flashlight Radar specifications is given below:

Flashlight Radar Specifications

Operating Frequency	35	GHz
Swept Bandwidth	1	GHz
Transmit Power	10	mW
Dynamic Range	> 55	dB
Linearity	0.4	dB
Channel Isolation	> 25	dB
Depth of Field	2 - 5	m
Range Resolution	15	cm
Spot Size Diameter	12	cm

The radar transmits alternate polarizations (horizontal and vertical, or right- and left-circular) by means of a waveguide switch. However, the radar can receive both polarizations simultaneously. The polarization basis (linear or circular) can be changed in hardware by using a polarizer; it can also be changed in software, as explained Section 6.3.1.

The radar head with antenna weighs about forty pounds; the antenna is removable so that other antennas with different beamshapes may be substituted. The millimeter-wave head and antenna are shown in Figure 3. Further information on the antenna is provided in Section 4.

The received signals are filtered and digitized in two 12-bit A/D converters, one for each receive channel. The digitized signals are stored in a portable computer for real-time individual processing. The original data is later transferred to a mainframe computer for image formation from the many returns of a whole target scan.

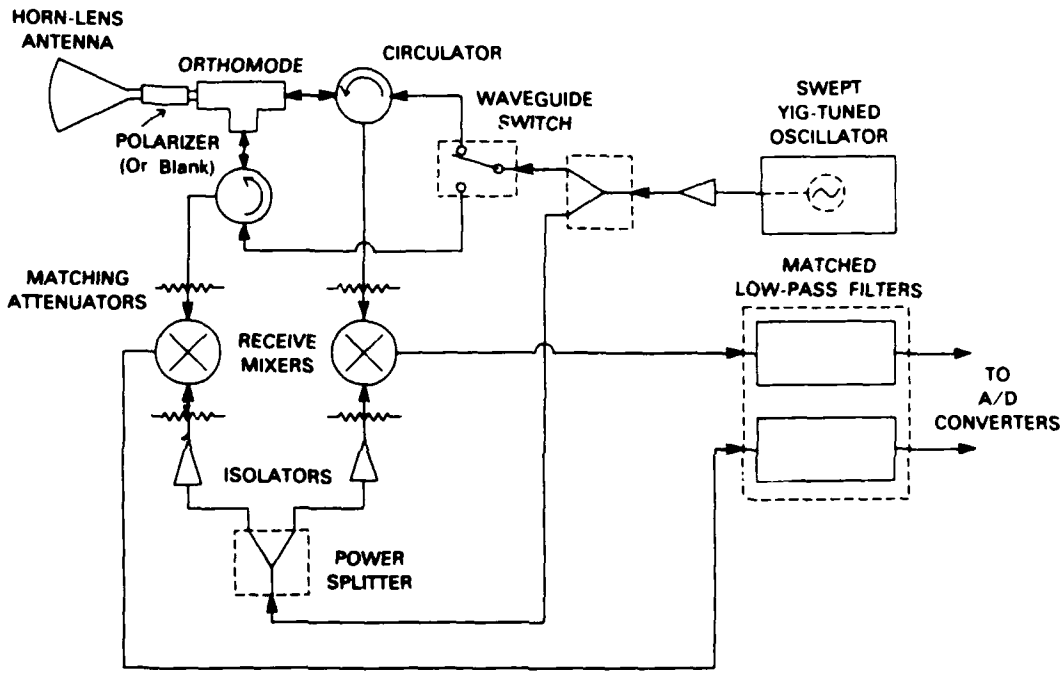

Figure 2: Detailed block diagram of Flashlight Radar system.

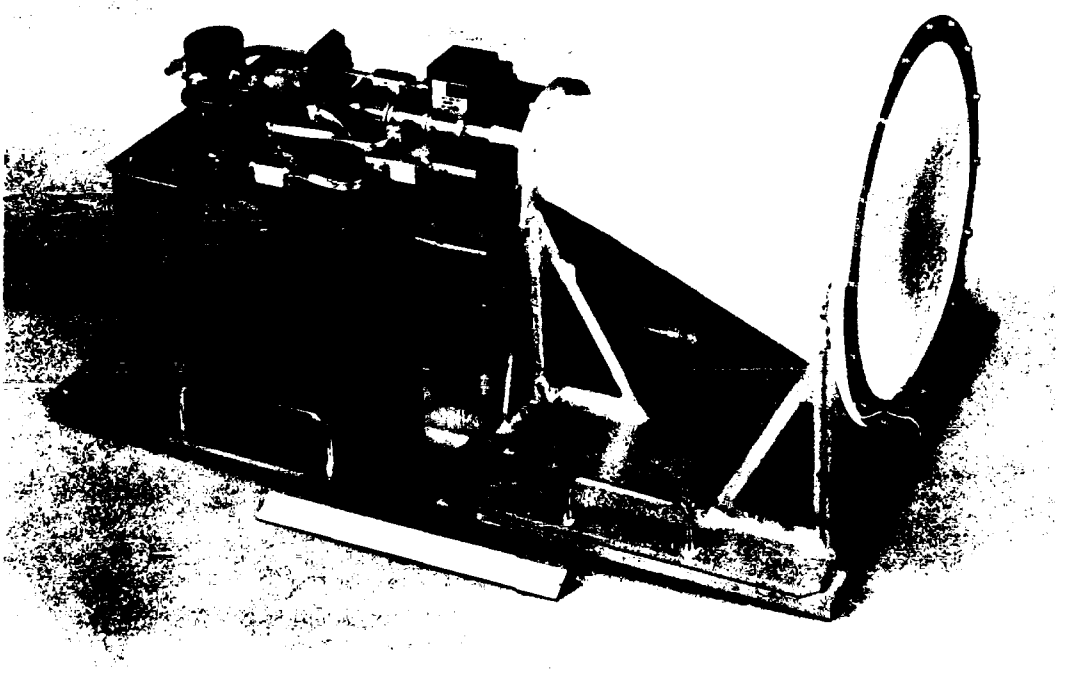

Figure 3: Flashlight Radar millimeter-wave electronics and antenna.

The portable computer also commands a small, custom-built control computer. This control computer operates the waveguide switch, as well as the radar's positioner. The positioner is similar to a small forklift. For horizontal translation, the positioner is pushed into place on flanged wheels that run on portable tracks. A video camera with date and time stamping is co-registered with the Flashlight Radar beam to provide a visual record during target scans.

3.1 Reference

1. R. Zoughi, L.K. Wu, and R.K. Moore, "SOURCESCAT: A Very-Fine-Resolution Radar Scatterometer." University of Kansas Remote Sensing Laboratory Technical Report RSL TR 5870-1.

4 Measured and Theoretical Antenna Performance

This section discusses the properties of the Flashlight Radar antenna. Measurements and a theoretical model are presented, giving insight into the spatial behavior of the focused radiation field.

4.1 Measurements

The Flashlight Radar uses a focused, scalar, horn-lens antenna [1]. The antenna is an Alpha Industries Model 858-12A-250/C that was modified according to Lincoln Laboratory specifications to produce a beam focused at 10 ft from the lens aperture. The purpose of focusing is to produce radiation fields in the Fresnel zone. This means that the fields near the focal plane are spherical TEM waves as ordinarily obtain in the far-zone (i.e., at distances $z > 2D^2/\lambda$, where D is the aperture diameter). The Flashlight Radar antenna produces a concentrated field over a small spot size. The co-polarized beam in the focal plane has a measured -3 dB spot size diameter (circularly symmetric) of 4.6 in. The focused-beam properties of the antenna give the radar high angle-angle (azimuth and elevation) resolution.

Antenna patterns in the E- and H-planes were measured by Alpha Industries at a variety of distances and frequencies. Two examples of these measurements can be seen in Figures 4 and 5, which show the E- and H-plane patterns at the focal distance (10 ft), at the radar center frequency (35 GHz). Cross-polarization is less than -33 dB on boresight, and the co-polarized sidelobes are less than -27 dB in the cardinal planes. The co-polarized -3 dB beamwidth is 2.15 ± 0.5 degrees from 8 ft to 15 ft in both planes. The antenna has excellent pattern symmetry and low cross-polarization, both are necessary for good performance with circular polarization.

4.2 Theory

In order to obtain additional insight into the behavior of the fields near the focal region, theoretical studies of antenna performance were undertaken. The exact on-axis electric field at 35 GHz, for the aperture focused at 3.05 m (10 ft) from the aperture, is shown in Figure 6. The results were obtained by numerical integration with the aperture field expressed as an HE_{11} mode with quadratic phase variation. The magnitude of the field at the aperture is unity, or 0 dB. The magnitude of the field near the aperture oscillates with distance until a peak is reached at 1.75 m. The electric field then decays approximately inversely with distance between 2 and 5 m (i.e., near the focal distance). Beyond 5 m, the field decays more strongly than inversely with distance (the function 4.4/range is shown in Figure 6 for comparison). The field does not begin to decay inversely with distance again until approximately 25 meters. (At 35 GHz, the far-field distance $2D^2/\lambda$ is 21.7 m.)

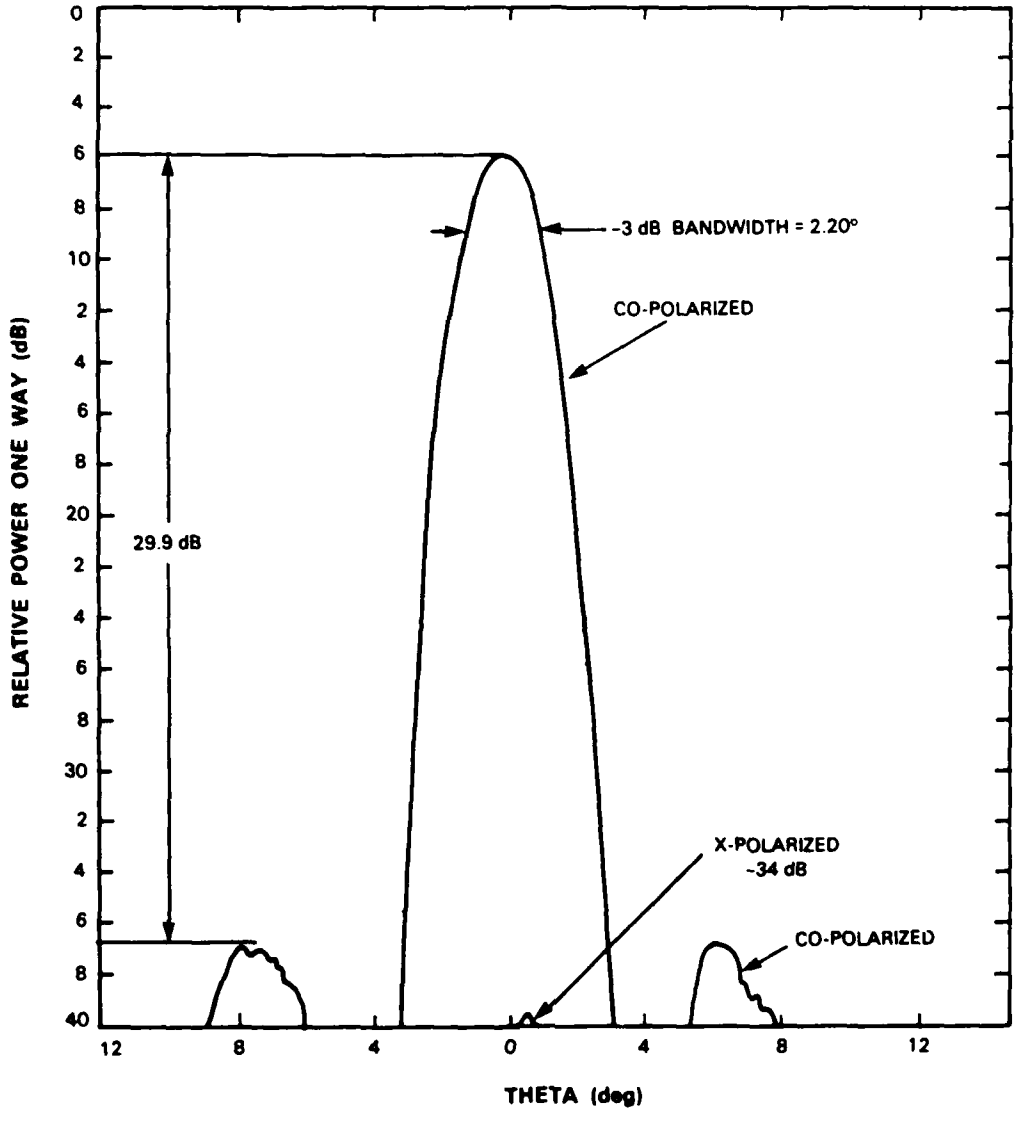

Figure 4: Measured E-plane patterns at 10 ft and 35 GHz.

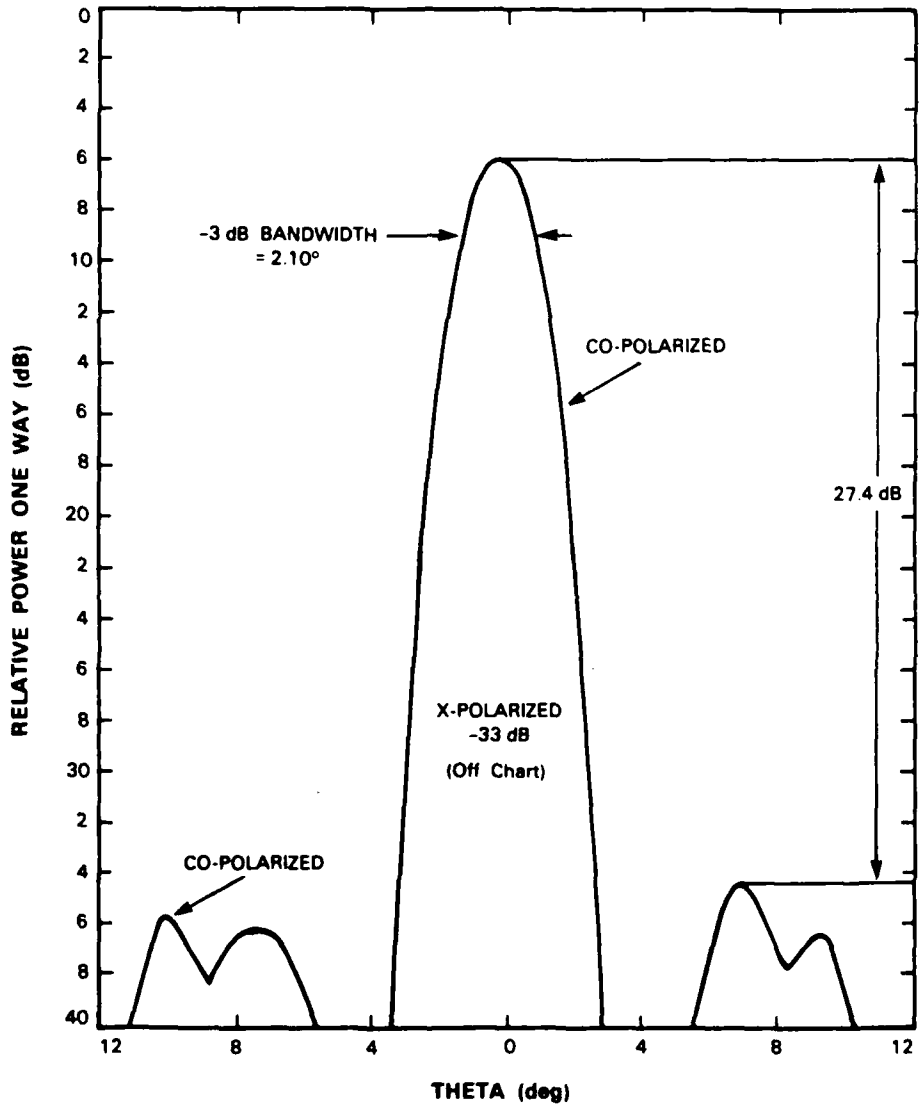

Figure 5: Measured H-plane patterns at 10 ft and 35 GHz.

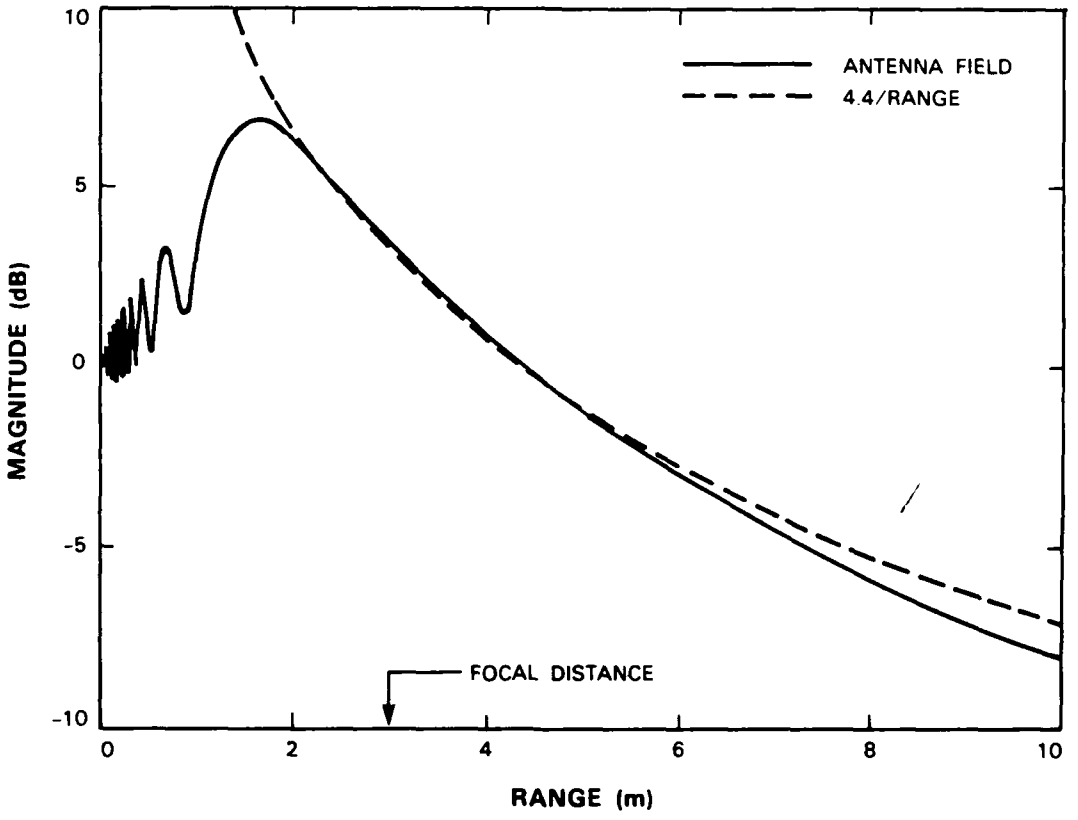

Figure 6: Theoretical on-axis electric field.

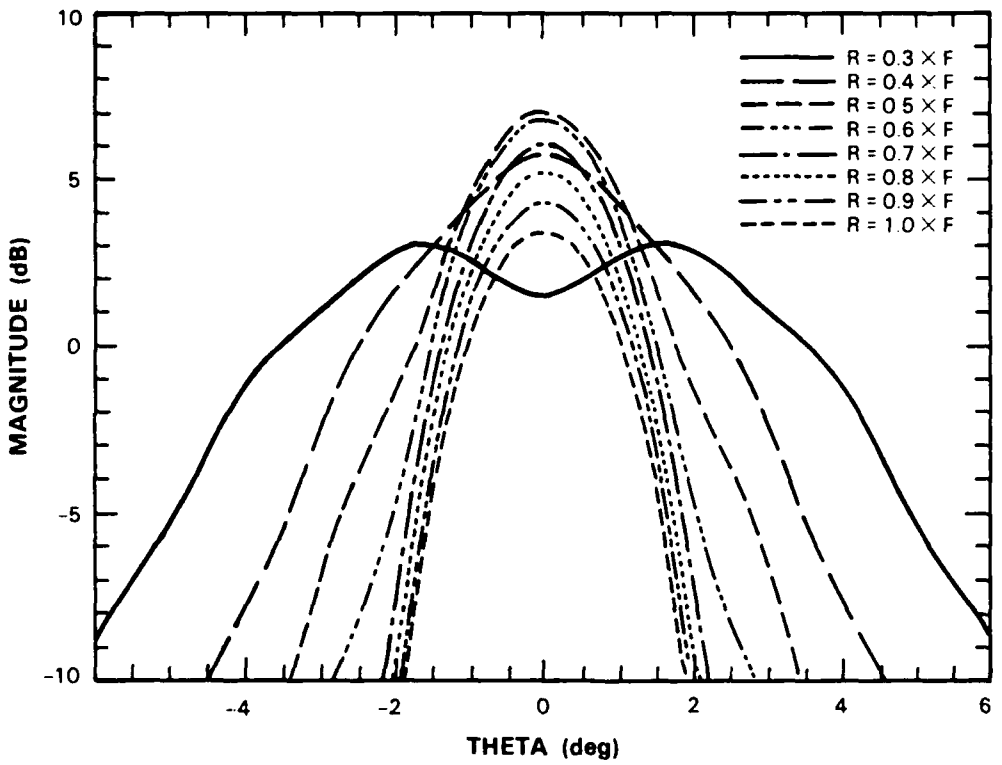

Figure 7: Theoretical E- or H-plane patterns (Fresnel approximation) at ranges up to the focal distance.

Figure 7 shows the behavior of the electric field as a function of polar angle, in the region from the lens aperture to the focal point. These results are based on the Fresnel approximation. The field at 0.3F ($\approx$ 3 ft) is bifurcated. A narrow beam is forming between 0.4F and 0.6F, and by 0.7F the beam has completely formed.

Figure 8 shows the behavior of the field, including the close-in sidelobes, in the range 1F to 3F. The amplitude patterns show the classical narrow-beam pattern at the focal distance. At the other distances, pattern degradation is seen in the form of a spreading mainlobe.

The results shown in Figures 6 and 7 can be used to generate the -3 dB beam cylinder profile for the Flashlight Radar. Figure 9 shows the beam cylinder profile from 4 ft to 30 ft. From the lens aperture to 4 ft, the field is not in the form of a narrow beam. From 4 ft to approximately 8 ft a well-defined beam cylinder can be seen. The beam cross section (spot size) varies between 2 and 3 in. over this range. Beyond 8 ft the field is spreading, with a well-defined beamwidth of 2 deg. The theoretical beam cross section is 3.5 inches at the focal distance of 10 ft.

Mathematical details of the antenna analysis are given in Appendix A.

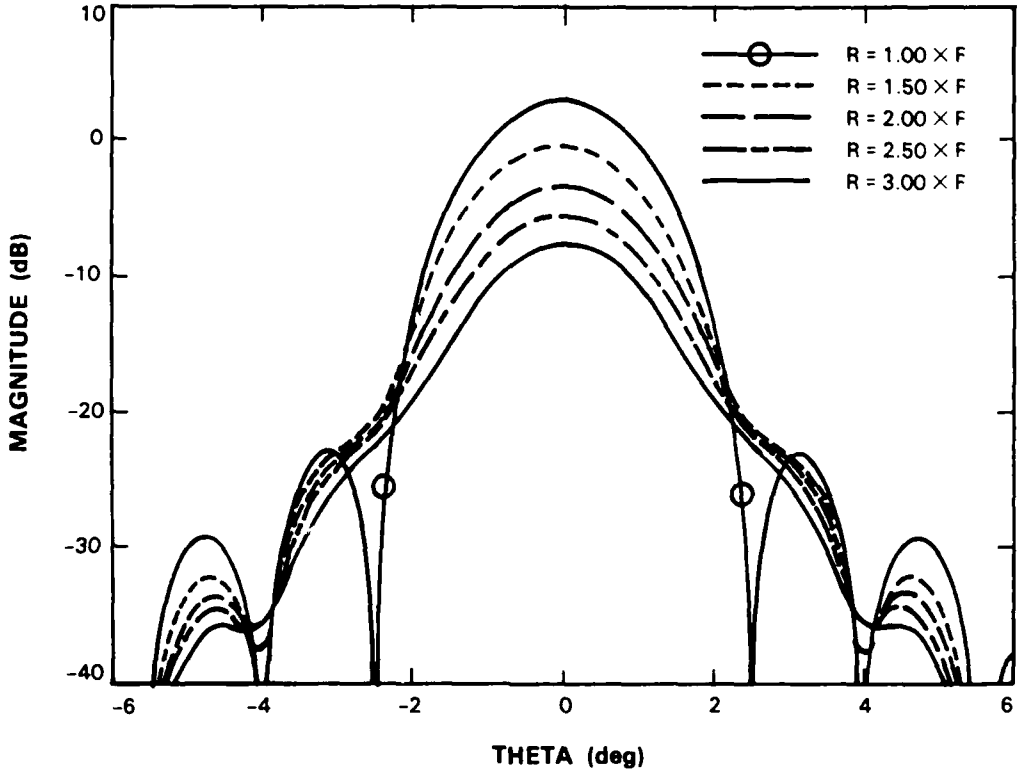

Figure 8: Theoretical E- or H-plane patterns (Fresnel approximation) in the range 1F to 3F.

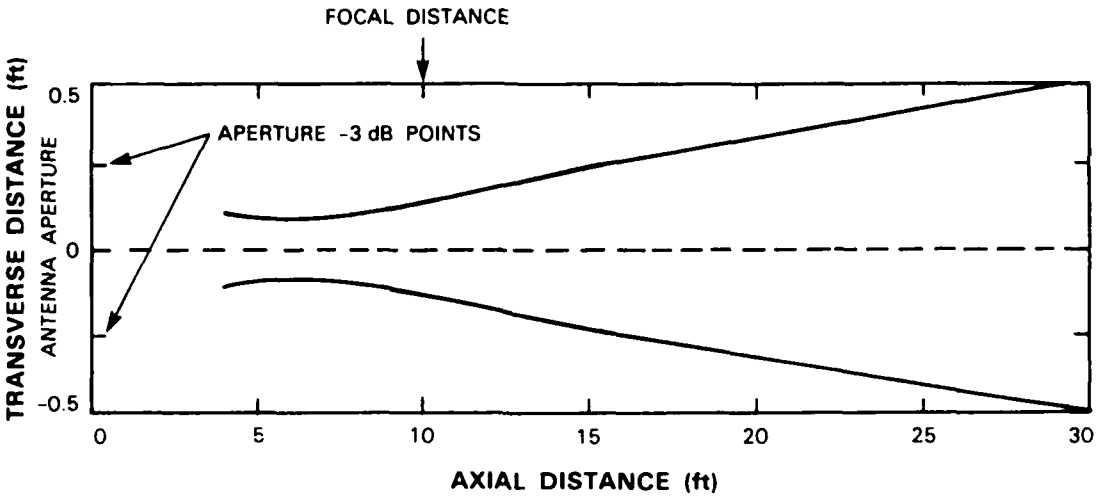

Figure 9: Theoretical −3 dB beam-cylinder profile.

4.3 Reference

1. D.J. Blejer, "Flashlight Radar Antenna Theory and Measurements", MIT Lincoln Laboratory, 29 February 1988, 47PM-ADT-0062.

5 Backscatter Theory and Measurements

This section discusses the properties of the Flashlight Radar as a scatterometer (an instrument for measuring radar cross section) [1] . RCS is directly measurable only under far-field, plane-wave conditions. Because the Flashlight Radar uses a focused beam, it does not measure RCS directly. The ability to measure RCS with the Flashlight Radar, taking into account the effects of using the focused-beam antenna, is achieved by combining theoretical modeling with measurements. A family of calibration curves are obtained and then incorporated into the radar signal processing software.

5.1 Theory

The power returned to the Flashlight Radar from a target can be computed using a Reaction integral formulation [2]. The particular formulation used here is derived from an equation obtained by Hu for computing the power transfer between two antennas in the near zone [3]. By invoking the Induction Theorem [4], a scatterer can be treated as a transmitting antenna, and the radar as a receiving antenna. Thus the general monostatic scattering problem is equivalent to the general two-antenna problem.

The Induction Theorem can be used to compute the ratio of received power to transmitted power for the Flashlight Radar illuminating a perfectly conducting circular disk. Figure 10 shows the ratio of the power received from an on-axis circular disk to the power transmitted, as a function of distance from the Flashlight Radar, for several disk sizes (the limiting case of the infinite plate is also shown). The curve for the 1 cm disk resembles the square of the on-axis antenna field (see Figure 6). The curves for the larger disks begin to resemble the curve for an infinite plate.

The curves of Figure 10 can be used to determine how well the Flashlight Radar can measure the RCS of the disks directly – without any special processing. For example, if a 3 cm radius disk at the focal point (3 m) is used to calibrate the Flashlight Radar in dBsm, how accurate will the RCS measurements for the other disks be? This can be determined by dividing the curves of Figure 10 by the RCS of the disks and multiplying by range to the fourth power:

$$\left(\frac{P_r}{P_t}\right)' = \frac{\lambda^2 R^4}{4\pi^3 a^4} \cdot \frac{P_r}{P_t} \tag{1}$$

where λ is wavelength, R is range, and a is disk radius.

The resulting curves of normalized power ratio are shown in Figure 11. The variations among the curves indicate the errors that are introduced into an RCS measurement. Under far-field conditions the curves would reduce to a single value; at the focal distance the RCS measurement of the 1 cm radius disk would be in error by ≈ 0.8 dB, and the error for the 5 cm disk would be ≈ -1.8 dB (both based on calibration using the 3 cm disk at the focal distance). The errors are less at the farther ranges, provided the calibration is done at those

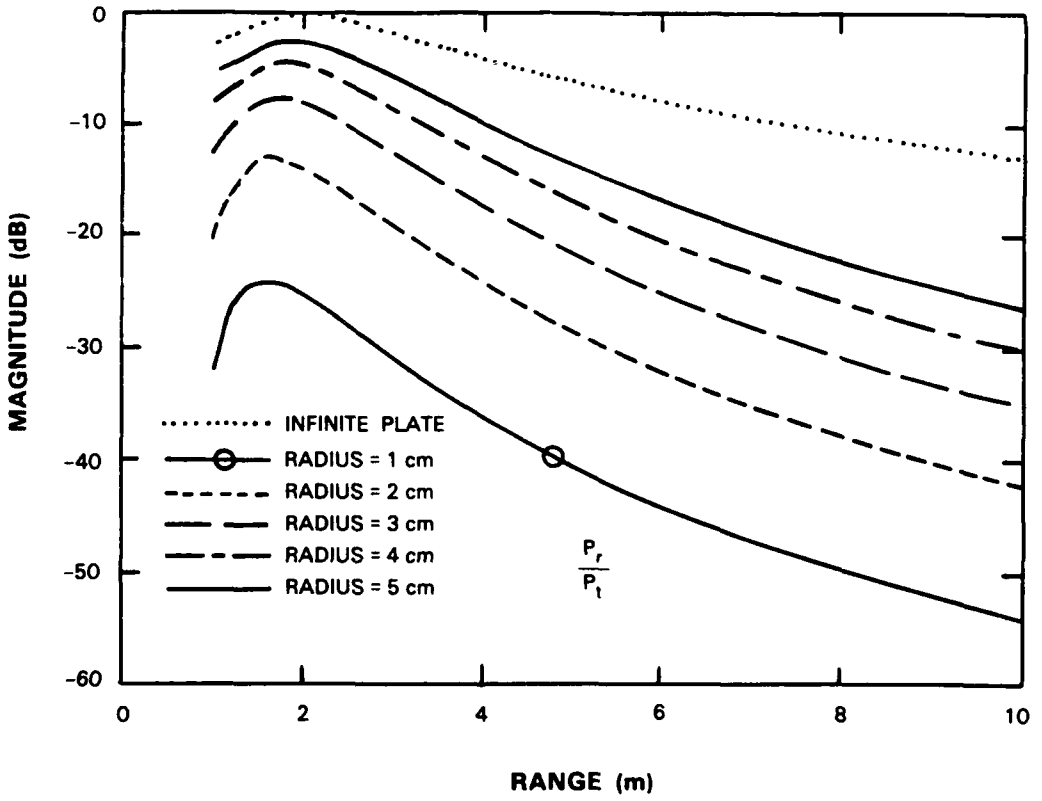

Figure 10: Theoretical power ratios from circular disks.

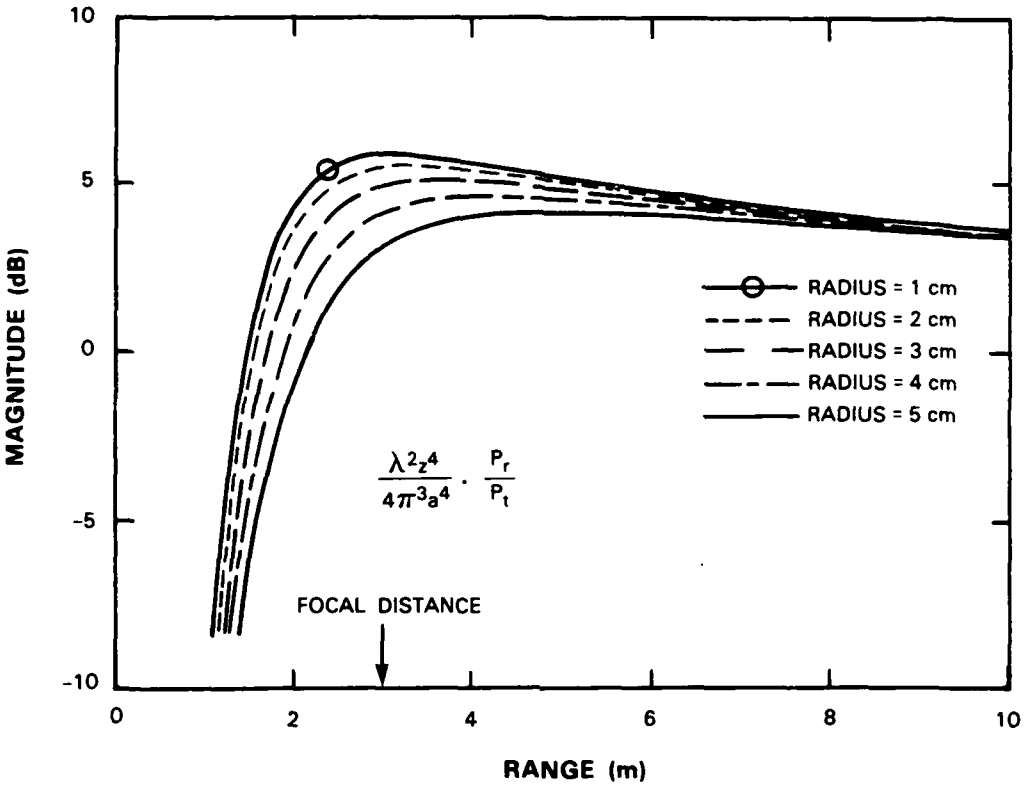

Figure 11: Theoretical normalized power ratios from circular disks.

ranges. Figure 11 shows that the focal region is the poorest region in which to perform calibration; nonetheless, the errors for the 5 disks would be within $\pm$ 1.5 dB for ranges greater than the focal distance.

A calibration curve which is simply the multiplicative inverse of the 1 cm curve is incorporated into the Flashlight Radar signal processing. This corrects for RCS variation with range. Mathematical details of the underlying backscatter theory are given in Appendix B.

5.2 Measurements

Measurements of two disks with radii of 2.8 cm and 5.0 cm were made with the Flashlight Radar at ranges from 1 to 6 m. The backscattered powers are shown in Figure 12, and the normalized backscattered powers in Figure 13. Since transmitted power was not measured, the results are shown in dB relative to the peak value. Figure 12 shows both the HH and VV channels; small differences ($\leq$ 0.5 dB) between the two channels reflect errors in polarimetric calibration. The ripples in Figures 12 and 13 are due to errors in aligning the disks. Nonetheless, the measured results compare favorably with the theoretical predictions

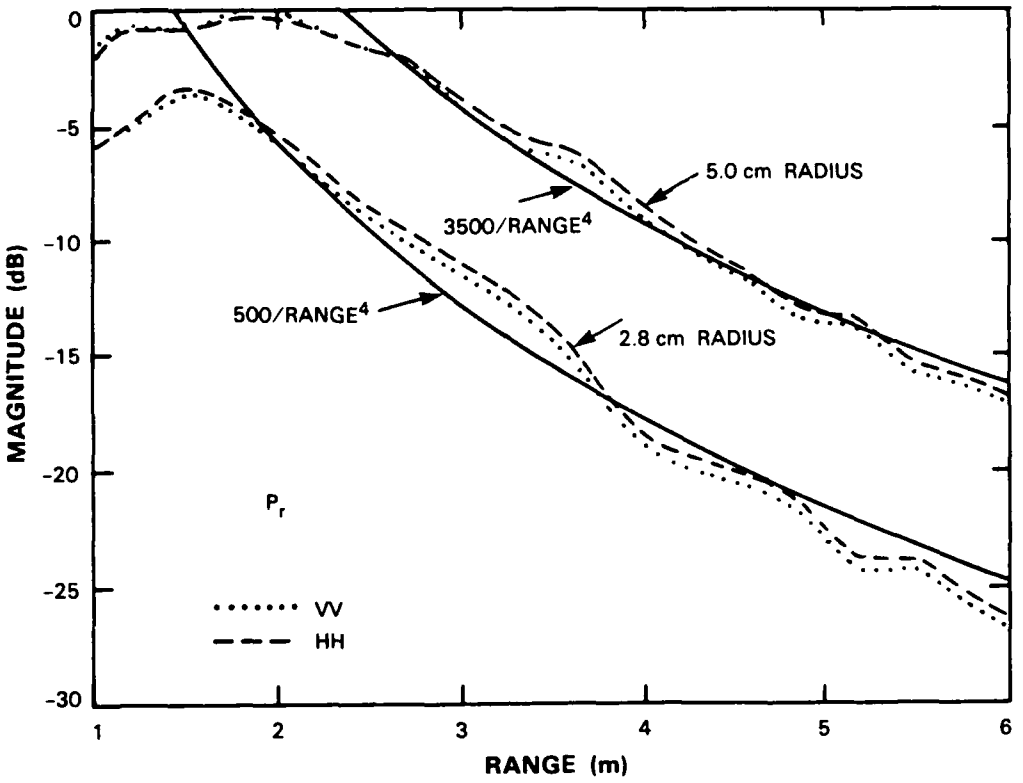

Figure 12: Measured backscattered power from circular disks.

shown in Figure 11.

Similar measurements will be made with trihedrals and spheres. Neither of these targets is alignment-sensitive, so the data should be free of ripples.

5.3 References

1. D.J. Blejer and S.M. Verbout, "Flashlight Radar Backscatter Theory", MIT Lincoln Laboratory, 13 April 1988, 47PM-ADT-0064.

2. V.H. Rumsey, "Reaction Concept in Electromagnetic Theory", Physical Review, 15 June 1954, Volume 94, Number 6, pp. 1483-1491.

3. Ming-Kuei Hu, "Near-Zone Power Transmission Formulas", IRE National Convention Record, 1958, pp. 128-138.

4. R.F. Harrington, Time-Harmonic Electromagnetic Fields, 1961, McGraw-Hill, Section 3-7.

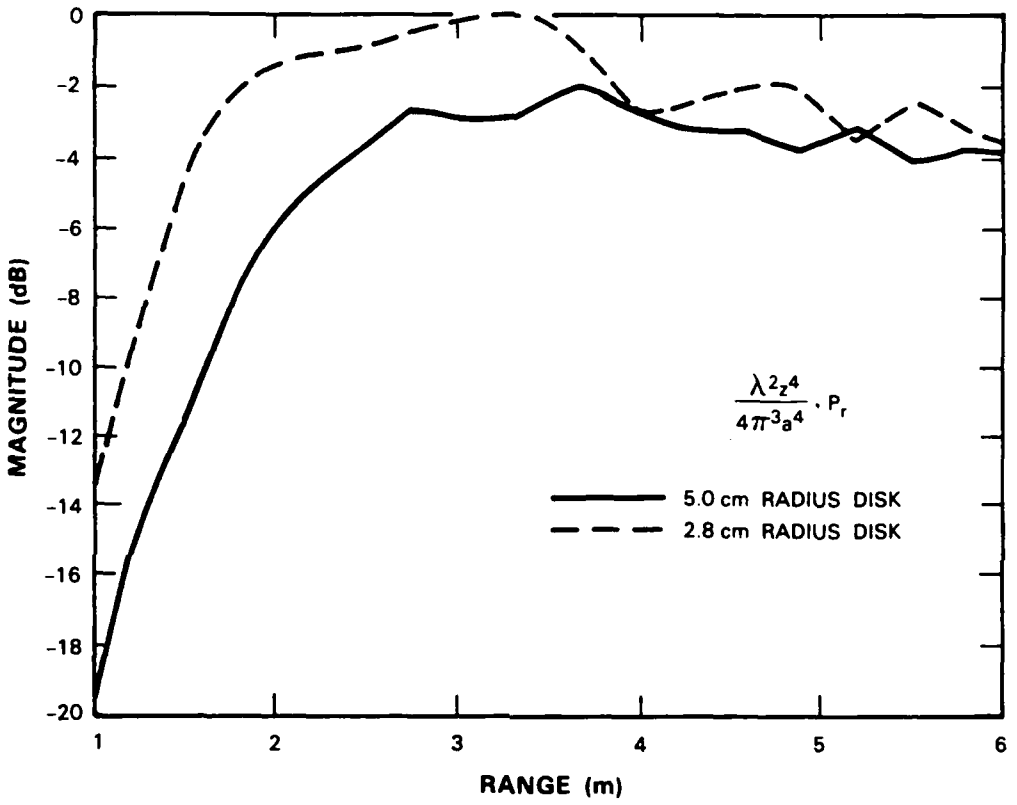

Figure 13: Normalized measured backscattered power from circular disks.

6 Data Processing

This section discusses the polarimetric calibration, signal processing, and image formation procedures used to convert the raw Flashlight Radar data into the final output.

6.1 Polarimetric Calibration and Compensation

The Flashlight Radar measures the polarization scattering matrix (PSM) (a complex, symmetri two-by-two matrix) of targets of interest. Hardware imperfections result in polarimetric distortion of two types: (1) crosspolarization leakage, and (2) mismatches in gain or phase between pairs of the four channels (a polarimetric channel corresponds to an element of the PSM). The objective of polarimetric calibration and compensation is to measure and remove the effects of polarimetric distortion.

A mathematical definition of polarimetric distortion is given in Barnes [1]; it is shown that distortion can be described by

$$E = zB^T\, A\, C \tag{2}$$

where A is the true form of the PSM, B and C are the one-way distortion matrices of the receive and transmit antennas, respectively, E is the measured (distorted) PSM, and z is a complex constant which includes the effects of two-way propagation.

The distortion matrices B and C are complex, two-by-two matrices which are not necessarily symmetric. In perfectly passive, reciprocal systems, it can be shown that $B = C$; however, the Flashlight Radar includes circulators, which are nonreciprocal devices. Thus we cannot assume that B and C are equal.

The objective of the calibration and compensation effort is to estimate the distortion matrices B and C, and then to pre- and post-multiply the distorted matrix E by the inverses of their estimates: $\hat{A} = (\hat{B}^T)^{-1} E \hat{C}^{-1}$. If we do a good job of estimating the distortion matrices, then $\hat{A}$ will be equal to A.

The technique for estimating B and C is to measure the distorted PSMs for a trihedral, a dihedral with horizontal crease, a dihedral with its crease at 45 deg with respect to horizontal, and a gridded trihedral. This last target consists of a trihedral with a parallel-wire grid stretched across its mouth; the wires are at a 45 deg angle with respect to horizontal. By using appropriate ratios of pairs of elements from the distorted PSMs, the elements of B and C can be unambiguously estimated using techniques given by Barnes [1, 2].

B and C matrices calculated with this technique were checked against those found the using techniques of Wood [3], and were found to be in excellent agreement.

Using Barnes's calibration technique, it was found that the cross-polarization leakage of the radar is fairly good (-25.3 dB), and can be ignored with no significant loss of accuracy. Also, the gain mismatches (of the vertical channel with respect to the horizontal channel)

on transmit and receive are -0.7 dB and 1.6 dB, respectively, while the phase mismatches are -137 degrees and -121 degrees, respectively.

So far, we have addressed relative polarimetric calibration, which calculates the elements of the B matrix normalized by B_{11}, and the elements of the C matrix normalized by C_{11}. Absolute calibration involves estimating the magnitude of $|B_{11}C_{11}|$. If a target is so large that it more than fills the beam, this magnitude will be underestimated, leading to an incorrect calibration. However, for targets which are small with respect to the beam, an R^{-4} dependence has been shown to describe range falloff (see Section 5). For this case, measuring the HH response of a single high-quality trihedral of known RCS serves to calibrate the absolute gain of the radar.

6.2 Signal Processing

The Flashlight Radar is a coherent radar that uses a linear FM chirp waveform with a bandwidth of 1 GHz. The receiver architecture features deramp-on-receive, in which the received signal is mixed with a delayed version of the transmitted chirp, resulting in a real, bipolar baseband signal.

The Flashlight Radar samples the baseband signal using a single A/D per receive channel. This is in contrast to typical coherent systems, which use separate A/Ds for the in-phase and quadrature signal components. Nevertheless, the Flashlight Radar is coherent.

To generate a fully polarimetric set of range profiles, 256 real samples are taken of each of the four polarimetric channels, in the linear basis (HH, HV, VH, and VV); each set of 256 samples is then Fourier transformed, and the negative frequencies are discarded. The result is a 128-bin complex range profile. (Note that due to the conjugate symmetry of the Fourier transform of a real signal, no information is lost by discarding the negative frequencies.)

In any actual radar system there are microwave hardware imperfections; therefore, the above process alone would not yield good results. Experiments with corner-reflector targets showed pre-deramp distortion, which increased the near-range sidelobes beyond their nominal value. Further corrections were needed.

A model of the pre-deramp distortion implies a method for its removal via software signal processing. To model the pre-deramp distortion, let the transmit chirp be

$$x_1(t) = \exp\{j2\pi(f_0 t + \frac{B}{2T}t^2)\}, \quad 0 \le t \le T \tag{3}$$

where f_0 is 35 GHz, B is 1 GHz, and T is 13 ms. The instantaneous frequency of the transmitted signal is then

$$f_1(t) = f_0 + \frac{B}{T}t \tag{4}$$

which varies from 34.5 to 35.5 GHz. The transmitted signal propagates to the target at range R and then back, with a round-trip time of $2R/c$. The signal is received by the antenna; it

then passes through an orthomode transducer and circulators, after which it is mixed with the deramp signal. The microwave network does not have a perfectly flat frequency response over the entire swept rf bandwidth (f_0 to $f_0 + B$). Let us denote its frequency response over this band by the complex function $\hat{a}(f)$; this function is complex in order to represent both the amplitude and phase distortion introduced by the microwave network.

Now we make an important approximation: we assume that the returned signal at any time within the chirp is a narrowband signal with an instantaneous center frequency $f_1(t - 2R/c)$. We assume further that the response of the pre-deramp microwave network to this signal at time t can be approximated by the network response to the instantaneous frequency at time t, which is

$$x_3(t) = a(t)x_2(t), \tag{5}$$

where $a(t)$ is a complex function of time; when $a(t)$ is evaluated at the RF frequency $f = f_1(t - 2R/c)$, it is equal to the function $\hat{a}(f)$.

Formally, $a(f)$ is a function of RF frequency. However, because the transmit signal is a chirp signal which linearly relates frequency to time, $a(f(t))$ itself can be viewed as a function of time. Hence, if we can determine the function $a(t)$, then we can divide it out of every phase history, and thus reduce the near-range sidelobes to their nominal value.

To determine the function $a(t)$ for a given polarization, we perform the following steps:

1. Measure the response of a dihedral or trihedral placed near the middle of the range of interest (i.e., at a range of 3-4 m).

2. Generate a range profile using the procedure outlined at the beginning of this section. Find the peak magnitude of this profile.

3. Circularly shift the range profile so that the peak is at DC (zero range).

4. Inverse-transform the shifted range profile using a 128-point IFFT. This produces the desired distortion function, which is stored for use in the processing described below.

5. Use the distortion function from Step 4 to compensate for the pre-deramp distortion. The steps are as follows:

   (a) Generate a range profile, using the procedure described at the beginning of this section.

   (b) Inverse-transform the range profile; this yields a 128-point complex phase history.

   (c) Weight the phase history using a Hamming function.

   (d) Divide the weighted complex phase history by the distortion function, and then FFT it.

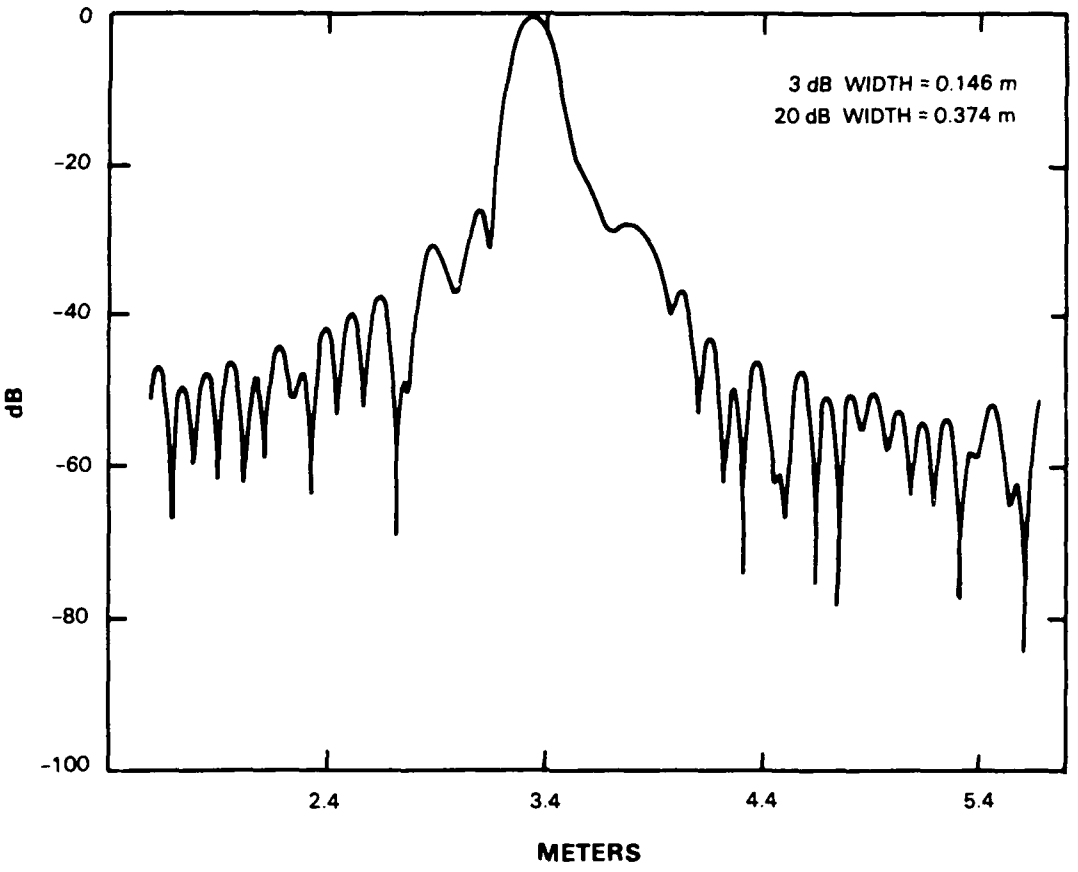

Figure 14: Range profile of point target, before correction.

6. Apply the distortion matrices B and C (see Section 6.1) to the range profile.

Figures 14 and 15 demonstrate the reduction in near-range sidelobes achievable by using this correction procedure. It is important to note that the distortion function for this example was derived from the same target and at the same range as was the range profile; therefore this example represents a best-case correction. Normally, one reference target (at the same range as the primary scatterer) will be used to generate a distortion function that is applied to all targets.

In experiments to date, the correction procedure has been found to work fairly well as long as the range to the reference target is within 1-2 m of the range to the primary scatterer in the range profile to be corrected. We are currently working to eliminate this limitation.

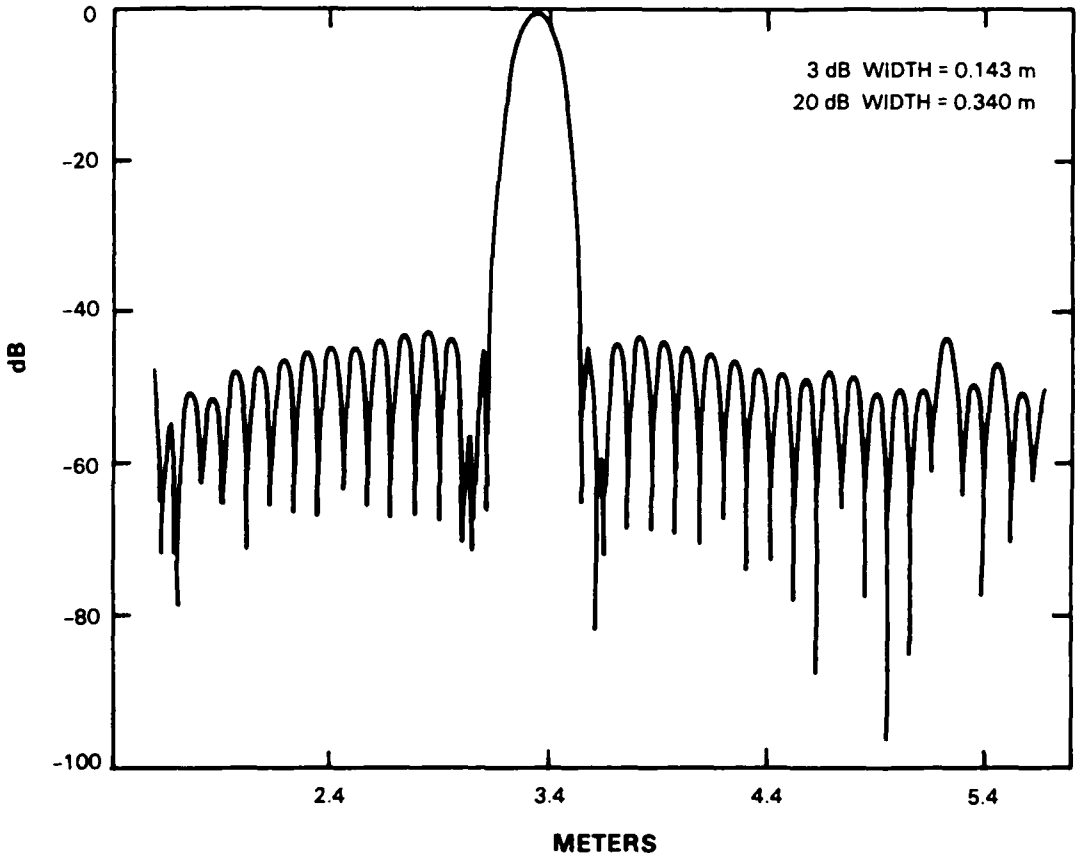

Figure 15: Range profile of point target, after correction.

6.3 Image Formation

There are two major steps in image formation for a target: (1) generating the range profile from each "snapshot" of the target, and (2) processing range profile information from contiguous snapshots to produce the desired images.

6.3.1 Generation of Range Profiles

The steps for generating range profiles are described in Sections 6.1 and 6.2. The results are range profiles corrected for both pre-deramp distortion and polarimetric distortion.

If desired, the profiles can be mathematically transformed from the linear polarimetric basis (HH, HV, VV, VH) to the circular polarimetric basis (LL, LR, RR, RL) by applying the following set of equations:

$$\begin{aligned} LL &= jHV + \frac{1}{2}(HH - VV) \\ LR &= j\frac{1}{2}(HH + VV) \\ RL &= j\frac{1}{2}(HH + VV) \\ RR &= jHV - \frac{1}{2}(HH - VV) \end{aligned} \tag{6}$$

6.3.2 Processing of Range Profiles

Overview

The input to this step is a set of range profiles representing a set of contiguous areas on the target. The 4.6-in spot size provides fine resolution in both azimuth and elevation. The measurements can be sequenced in any of the following ways:

1. A horizontal scan, which produces an image of a slice of the target at a particular elevation.
2. A vertical scan, which produces an image of a slice of the target at a particular cross-range location.
3. A two-dimensional (horizontal and vertical) raster scan, which produces a head-on image of the target.

In all three methods, a measurement is taken, then the sensor is moved one pixel width, then the next measurement is taken, and so on. This yields a number of adjacent looks at small portions of the target.

Processing Description

The Flashlight Radar offers considerable versatility in the kinds of images it produces. This is based on (1) a choice of data-collection modes (linear scan or raster scan), and (2) a choice of which data to present in the image (e.g., amplitude, phase, or range information). Such versatility is made possible by the three-dimensional capability of the Flashlight Radar. Three imaging methods are discussed below.

For a single linear scan (horizontal or vertical), each range profile in the data set is windowed to retain only the segment of the profile that represents the target range extent. These windowed segments may then be abutted sequentially in the direction of the scan. The resulting data array forms a two-dimensional image, in which the value of pixel (i, j) is the magnitude of the jth range bin in the ith profile of the sequence, and in which the pixel dimensions reflect the actual sample spacing in range and cross range.

For a raster scan, the range profiles are windowed in the same way as for a linear scan. One method of processing the windowed segments produces an image in which range is no longer one of the two image dimensions. Instead, the image is a "head-on" view of the target. In this kind of image, each pixel is associated with a "snapshot" of data from a small area of the target. The value of the pixel is the magnitude of the range bin at which the span $(|HH|^2 + |HV|^2 + |VV|^2 + |VH|^2)$ is a maximum. The pixels are always square, since the beam is circular. The truck tire image shown in Figure 18 was produced using this raster-scan technique.

Another way of processing raster-scan data produces an image in which range is plotted as a function of 2-D position. Specifically, for each "snapshot", the range at which the span is a maximum is plotted. This technique produces a three-dimensional perspective image which may actually resemble the physical target, as shown in Figure 19.

6.4 References

1. R. M. Barnes, "Polarimetric Calibration Using In-Scene Reflectors", MIT Lincoln Laboratory Project Report TT-65, 10 September 1986.

2. R. M. Barnes, "Polarimetric Calibration Using In-Scene Reflectors", 10th Annual DARPA-Triservice Symposium on Millimeterwaves, April 1986.

3. M. A. Wood, "A Calibration Procedure for a Coherent Scattering Matrix Radar", Royal Signals and Radar Establishment Memorandum 3889, May 1986.

7 Representative Experimental Results

This section presents the results of two experiments using the Flashlight Radar. The first is a measurement of dihedral and trihedral reflectors with and without radar camouflage. The second shows the instrument's three-dimensional capabilities as it measures the complicated scattering properties of a truck tire.

Reflectors and Camouflage

Camouflage is designed to absorb and scatter incident radar energy over a wide range of frequencies, blending the target into the background clutter. Typical radar camouflage netting is made from carbon fibers of varying lengths, randomly oriented in a plastic sheet. The sheet is cut so that the camouflage falls in a randomly folded manner when draped around a target or supported by tent poles.

Our experiment consisted of placing one or two layers of camouflage netting in dihedral and trihedral reflectors, and then illuminating them with the Flashlight Radar. The results are shown in Figure 16. Both attenuation and cross-polarization effects are detailed:

1. The two-way camouflage attenuation was about 12 dB per layer, with some variation due to the particular manner in which the material lay in the reflector.

2. The cross-polarization properties of the netting appear to be independent of the number of layers. For the dihedral reflector, the cross-polarization ratio was reduced by 19 dB; for the trihedral, the reduction in cross-polarization ratio varied between 5 and 9 dB, depending on the orientation of the netting. These results show that radar camouflage netting may confuse polarization-based classifier algorithms.

Truck Tire

The second experiment was a raster scan of a truck tire. The tire, shown in Figure 17, is a very complicated target: there are tilted dihedral structures in the hub cavities, radial spokes, bolt heads, interfaces between wheel and tire, and even a mud flap.

We performed the scan at an 11 deg depression angle, with the instrument pointed a few degrees off broadside. Selected results are shown in Figure 18 as intensity images presented in four polarizations. The polarizations are VV (linear co-polarized) and VH (linear cross-polarized), and LL (circular even) and LR (circular odd). (Data was collected in the linear basis, and mathematically transformed to produce the circular format images.) A physical outline of the tire is shown in the VV image. For each 3-in.-square pixel, we determined the range at which the span of the polarization scattering matrix was a maximum; the images in Figure 18 display the magnitudes of the returns (in the four channels) at that range.

FLASHLIGHT RADAR MEASUREMENTS
(Circular Basis)

NO. LAYERS	TWO-WAY ATTENUATION (dB)		CROSS-POLARIZATION RATIO (dB)	
	DIHEDRAL LL	TRIHEDRAL LR	DIHEDRAL RR/RL	TRIHEDRAL RL/RR
0	0	0	27	25
1	12	12	8	16
2	22	28	8	20

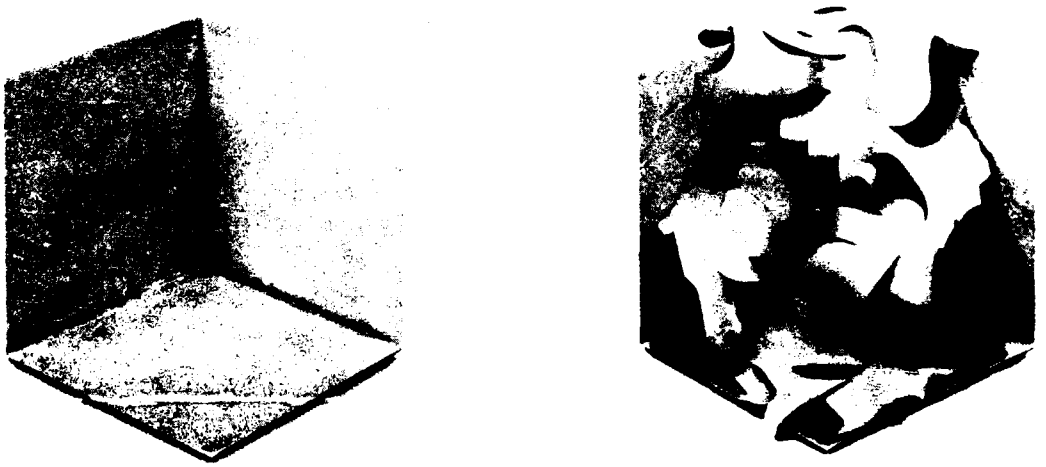

Figure 16: Effect of radar camouflage netting on returns from dihedral and trihedral reflectors.

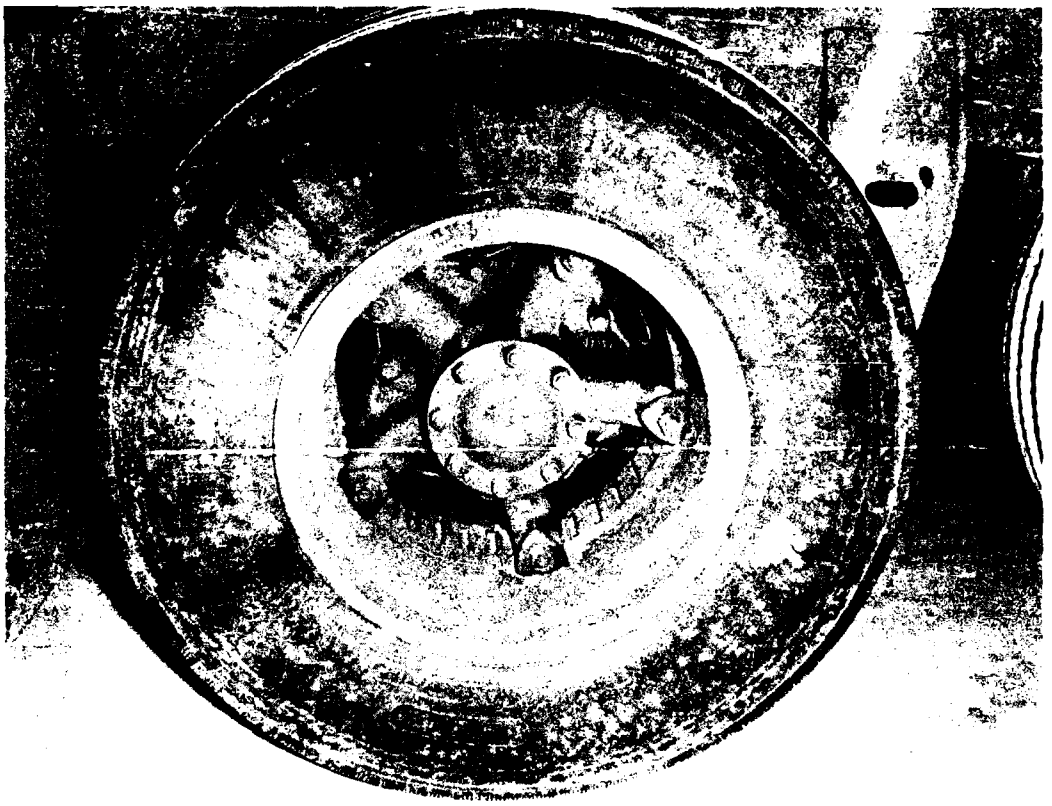

Figure 17: Truck tire.

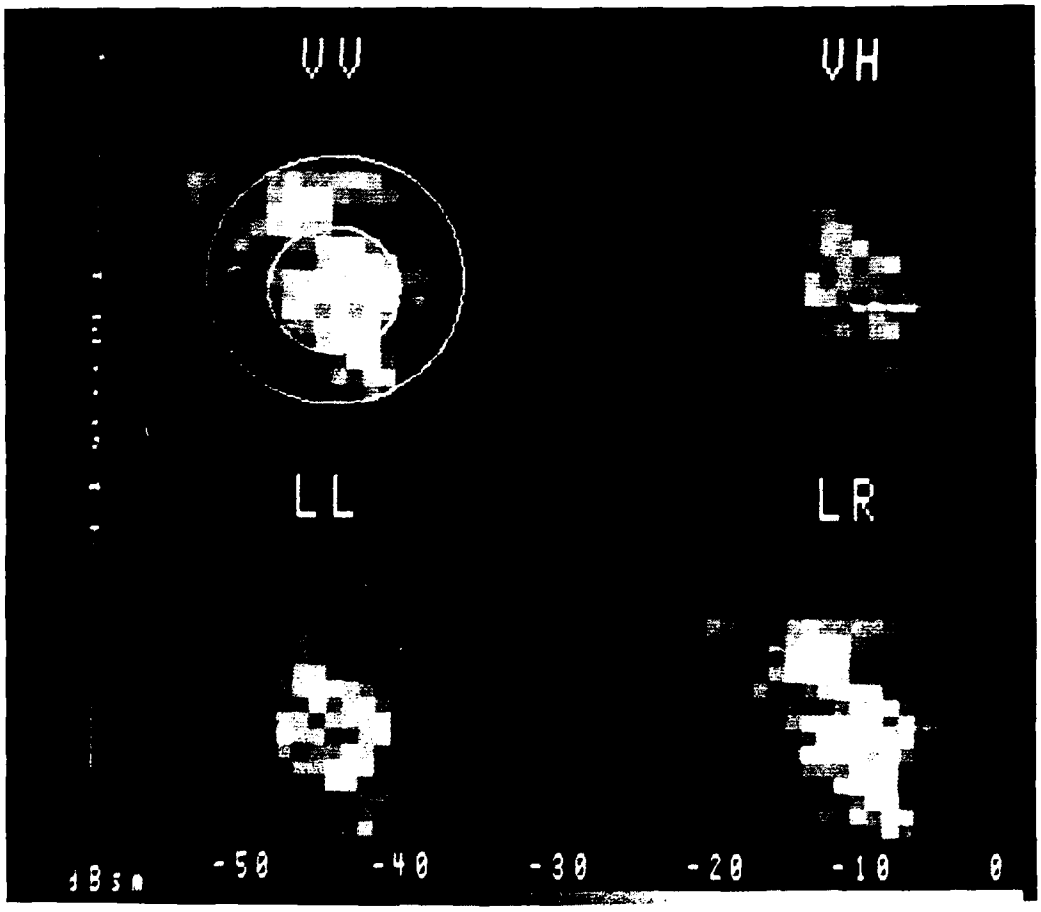

Figure 18: "Head-on" intensity image of truck tire. Pixel brightness indicates amplitude of return.

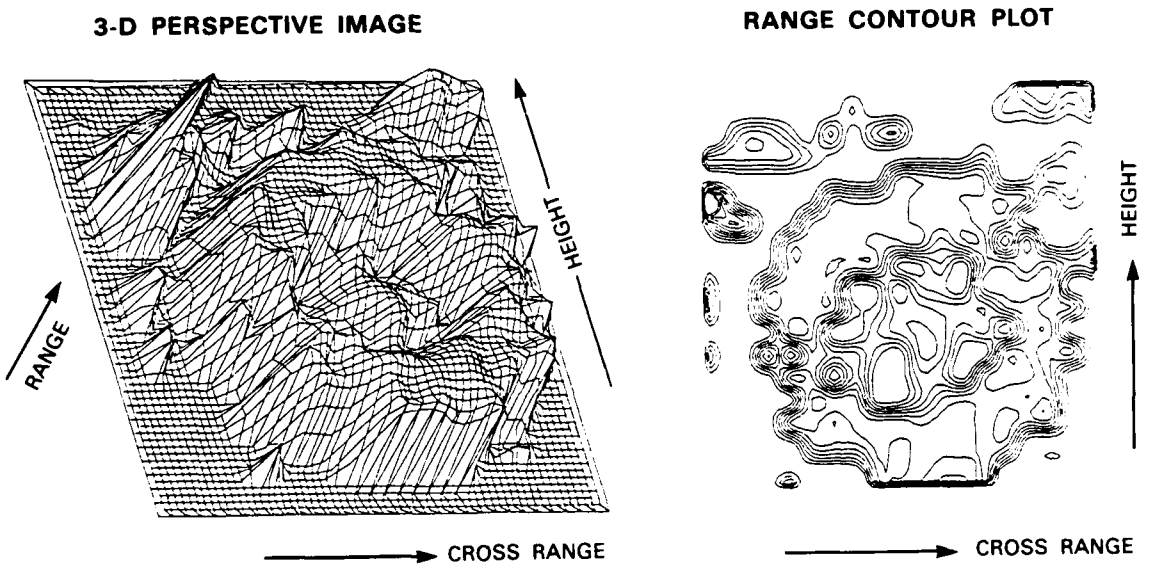

Figure 19: (a) Three-dimensional perspective image and (b) range contour plot of truck tire.

Three areas in the images are of particular interest:

1. The hub area is the brightest and most complex scatterer, with significant returns in all four channels shown, though the co-polarized (VV) and odd-bounce (LR) channels predominate.

2. The mud flap in the upper left hand corner is resolved from the tire.

3. There are strong echoes (in the VV and LR channels) from the vicinity of the rubber tire. At first, we surmised that these returns were a result of the radar energy going through the rubber and reflecting from the rear rim of the hub. In fact, however, the returns came from the tire surface; this can be seen in Figure 19a, which shows a 3-D perspective image of the tire. Further investigation revealed that the tire was steel-belted, with a layer of steel in the sidewall. Such a layer would produce primarily co-polarized and odd-bounce returns; Figure 18 clearly shows these characteristics.

   The range contour plot of Figure 19b shows details of the tire's hub structure, the tire outline, and the mud flap and other objects surrounding the wheel well.

8 Other Applications

We have used, or plan to use, the Flashlight Radar as an instrumentation-quality sensor to support a number of polarimetric investigations.

1. We have analyzed three-dimensional scans of complicated targets (such as the tread area of a tracked vehicle, or the cab structure of a truck), and have generated a number of polarimetric processing products. These include spatially localized polarization covariance matrices, pixel averages of RCS and span, and odd/even ratios.

2. We have studied the polarimetric transmission, absorption, and reflection properties of radar-absorbing materials (RAM). These materials include radar scattering nets and conformal RAM.

3. We will investigate the local polarimetric properties of natural clutter, such as foliage, snow, and mud. The instrument's translational raster-scan capability will enable us to gather data over an area large enough to encompass an entire tree or bush.

4. We have measured scale models of military vehicles and aircraft, and small military targets such as mines.

5. We will form three-dimensional SAR images of complicated targets (*i.e.*, involving multiple-scatter phenomena). For this application, the focused antenna will be replaced by a small broad-beam antenna, and the radar will be translated in two dimensions by a precision industrial positioner. Three-dimensional FFT processing will be used to form the images.

Appendices

A Antenna Modeling

The Flashlight Radar antenna field is modeled in this appendix. No attempt is made to model the antenna itself highly accurately, as this would require synthesizing the antenna aperture distribution. Rather, the antenna aperture distribution is postulated based on known properties of scalar-horn antennas. This approach was taken with the ADTS antenna [1], and found to give sufficiently good results to correctly describe the behavior of the antenna.

A.1 Analysis

The aperture electric field of a corrugated conical horn may be expressed as a simple HE_{11} mode in terms of the zeroth-order Bessel function [2], i.e.,

$$E_x^A(\rho', \psi') = J_o(\kappa\rho')e^{jk_o\alpha\rho'^2} \tag{7}$$

In this expression, the aperture electric field is assumed to be polarized in the x-direction, κ is the mode wavenumber, α is a constant that will be determined from the focal distance, and ρ' and ψ' are the source point variables in polar coordinates. The assumed aperture distribution is circularly symmetric, which produces equal E- and H-plane patterns.

Using the magnetic current formulation [3], the electric field in the Fresnel zone radiated by an x-polarized aperture distribution is given by

$$\vec{E}(\vec{r}) = \frac{jk_o e^{-jk_o r}}{2\pi r}(\hat{\theta}\cos\phi - \hat{\phi}\sin\phi) \int\int_{S'} E_x^A(\rho', \psi') e^{jk_o[\hat{r}\cdot\vec{\rho}' - \rho'^2/2r + (\hat{r}\cdot\vec{\rho}')^2/2r]} dS' \tag{8}$$

Substituting Equation (7) into Equation (8) yields

$$\vec{E}(\vec{r}) = \frac{jk_o e^{-jk_o r}}{2\pi r}(\hat{\theta}\cos\phi - \hat{\phi}\sin\phi) \int\int_{S'} J_o(\kappa\rho') e^{jk_o\alpha\rho'^2} e^{jk_o[\hat{r}\cdot\vec{\rho}' - \rho'^2/2r + (\hat{r}\cdot\vec{\rho}')^2/2r]} dS' \tag{9}$$

The focal distance F determines the quadratic phase coefficient α as:

$$jk_o\alpha\rho'^2 = jk_o\rho'^2/2F \Rightarrow \alpha = 1/2F \tag{10}$$

Therefore

$$\vec{E}(\vec{r}) = \frac{jk_o e^{-jk_o r}}{2\pi r}(\hat{\theta}\cos\phi - \hat{\phi}\sin\phi)\int\int J_o(\kappa\rho')e^{jk_o[\hat{r}\cdot\vec{\rho}' + \frac{\rho'^2}{2}(\frac{1}{F}-\frac{1}{r}) + \frac{(\hat{r}\cdot\vec{\rho}')^2}{2r}]}\rho' d\rho' d\psi' \quad (11)$$

where

$$\hat{r}\cdot\vec{\rho}' = \rho'\sin\theta\cos(\phi - \psi') \quad (12)$$

At the focal distance, the middle term in Equation 11 is zero, and the third term is small, i.e.,

$$\frac{(\hat{r}\cdot\vec{\rho}')^2}{2r} \leq \frac{a^2}{2F} \quad (13)$$

where a is the aperture radius (for the Flashlight Radar antenna, $a^2/2F = 0.0038$). Thus, the Fresnel field near the focal point resembles a Fraunhofer or far-field.

The Fresnel approximation (8) is usually valid beyond a few aperture radii from the aperture plane. The point of validity can be determined by computing the exact field on-axis and comparing it with the Fresnel field.

The exact electric field produced by a magnetic surface current [4] is given by

$$\vec{E}(\vec{r}) = \int_{S'} \vec{M}_s(\vec{r}') \times \nabla G \, dS' \quad (14)$$

The equivalent magnetic surface current is obtained from the aperture electric field via

$$\vec{M}_s = -2\hat{z} \times \vec{E}^A \quad (15)$$

$$= -2\hat{y}E_x^A \quad (16)$$

where the axial direction is the positive z-axis, G is the free space Green's function given by

$$G(\vec{r},\vec{r}') = e^{-jk_o R}/4\pi R \quad (17)$$

and R is the distance between the field-point and source-point variables, i.e.,

$$R = |\vec{r} - \vec{r}'| \quad (18)$$

Using

$$\nabla G = -(jk_o + 1/R)G\hat{R} \quad (19)$$

the exact electric field on-axis is given by

$$\vec{E}(0,0,z) = \frac{1}{2\pi}\int_{S'} E_x^A(\rho',\psi')(\frac{jk_o}{R^2}+\frac{1}{R^3})(\hat{x}z+\hat{z}x')e^{-jk_oR}dS' \quad (20)$$

$$= \hat{x}z\int_0^a J_o(\kappa\rho')(\frac{jk_o}{R^2}+\frac{1}{R^3})e^{-jk_o(R-\rho'^2/2F)}\rho' d\rho' \quad (21)$$

where

$$R = \sqrt{\rho'^2+z^2} \quad (22)$$

The exact electric field on-axis has only a co-polarized component (x-component). Because we have used the magnetic-current formalism, no longitudinal (z-component) electric field is obtained. A longitudinal electric field requires an electric charge distribution as a source; for the magnetic source described by Equation (15) the associated electric charge distribution is zero. There is, however, a nonzero magnetic charge distribution that produces a longitudinal magnetic field. This field component is only significant in the reactive near field and is, therefore, not of concern here.

A.2 References

1. D.J. Blejer, R.M. Barnes, and G.J. Gill, "ADTS Antenna/Radome Study", MIT Lincoln Laboratory, 13 August 1987, Project Report TT-69, ESD-TR-87-060.

2. R.J. Wylde, "Millimetre-Wave Gaussian Beam-Mode Optics and Corrugated Feed Horns", IEE Proceedings, Vol. 131, Part H, No. 4, August 1984, pp. 258-262.

3. R.E. Collin and F.J. Zucker, Antenna Theory, McGraw-Hill, 1969, Section 3.7.

4. G.J. James, Geometrical Theory of Diffraction for Electromagnetic Waves, Peter Peregrinus Ltd., 2nd Edition, 1980, Section 2.1.2.

B Reaction Formulation

The mathematical formalism for computing the backscattered power from a target illuminated by the Flashlight Radar is derived in this Appendix.

B.1 Derivation of Backscattered Power Equation

Consider two antennas arbitrarily oriented and separated from each other. Let Antenna 1 be transmitting and Antenna 2 be receiving. Then the ratio of received power to transmitted power [4] is given by

$$\frac{P_r}{P_t} = \frac{|\int_S (\vec{E}_2 \times \vec{H}_1 - \vec{E}_1 \times \vec{H}_2) \cdot \hat{n} dS|^2}{4[\mathrm{Re}\int_{S_1} (\vec{E}_1 \times \vec{H}_1^*) \cdot \hat{n}_1 dS_1][\mathrm{Re}\int_{S_2} (\vec{E}_2 \times \vec{H}_2^*) \cdot \hat{n}_2 dS_2]} \tag{23}$$

where S_1 is the transmitting-antenna aperture, S_2 is the receiving-antenna aperture, and S is an arbitrary surface between and including the two antenna apertures. The fields $\vec{E}_m$ and $\vec{H}_m$ are produced by Antenna m ($m = 1$ or 2) while transmitting. The two terms in the denominator are from Poynting's Theorem and are proportional to the power radiated by each antenna. The integral in the numerator is of the Reaction type and is proportional to the product of the received power and the power that would be transmitted by the receiving antenna if it were transmitting (this interpretation is illustrated in Appendix A with a very simple model).

Now consider the radar problem with a target arbitrarily close to the radar. Equation (23) can be modified and applied to this situation as follows: the fields radiated by the radar excite surface currents on the target; these currents may be treated as a transmitting antenna with the radar as the receiving antenna. If P_r/P_t is computed from Equation (23), then the interpretation of this quantity is the ratio of received power to scattered power. To obtain the ratio of received power to transmitted power, Equation (23) must be multiplied by the scattered power and divided by the transmitted power.

Changing notation so that superscript a refers to the radar antenna-aperture field and superscript s refers to the scattered field, the ratio of received power to transmitted power is given by

$$\frac{P_r}{P_t} = \frac{|\int_{S_a} (\vec{E}^a \times \vec{H}^s - \vec{E}^s \times \vec{H}^a) \cdot \hat{n}_a dS_a|^2}{4[\mathrm{Re}\int_{S_a} (\vec{E}^a \times \vec{H}^{a*}) \cdot \hat{n}_a dS_a]^2} \tag{24}$$

Equation (24) can be simplified by using the following two approximations:

$$\vec{H}^a \approx \hat{n}_a \times \vec{E}^a/\eta_o \tag{25}$$

$$\vec{H}^s \approx \hat{r}_s \times \vec{E}^s/\eta_o \tag{26}$$

$$\approx -\hat{n}_a \times \vec{E}^s/\eta_o \tag{27}$$

where η_o is free-space impedance. The first approximation relates the aperture magnetic field to the aperture electric field via free-space plane-wave relations. This is a standard approximation in aperture antenna theory for antennas that are well matched to free space. The second approximation relates the scattered magnetic and electric fields near the Flashlight Radar (see Appendix B.3), and is valid for targets that are at least a few aperture diameters away from the radar.

Using Equations (25) and (27) reduces Equation (24) to

$$\frac{P_r}{P_t} \approx \frac{|\int_{S_a} \vec{E}^a \cdot \vec{E}^s dS_a|^2}{(\int_{S_a} |\vec{E}^a|^2 dS_a)^2} \tag{28}$$

Equation (28) is readily interpretable. The scattered field that appears at the Flashlight Radar antenna aperture is weighted by the transmitting-aperture field. That is, the numerator proportional to the co-polarized received power times the transmitted power. The denominator is proportional to the square of the transmitted power.

B.2 Calculation of Power Ratio

Equation (28) was evaluated for the case of a circular disk on-axis from the Flashlight Radar and oriented normal to the radar-line-of-sight (RLOS). The aperture electric field was expressed analytically and the denominator was evaluated in closed form. The back scattered field was computed numerically by: (1) computing the field incident on the disk surface, (2) computing the Geometrical Optics (GO) reflected field on the disk surface, and (3) computing the back scattered field by using the GO reflected field as an equivalent aperture field.

B.2.1 Incident Field

The field radiated by the Flashlight Radar and incident on the disk is calculated by the method given in Appendix A.

B.2.2 Backscattered Field and Power Ratio

The reflected field is obtained from the incident field by

$$\vec{E}^r = (2\hat{n}\hat{n} - \mathbf{I}) \cdot \vec{E}^i \tag{29}$$

where $\hat{n}$ is the normal vector at the disk surface. The reflected field is used as an aperture field in Equation (8) to compute the backscattered field at the Flashlight Radar. Equation (28) is then evaluated to obtain the ratio of received power to transmitted power. The procedure outlined in this Appendix for obtaining the power ratio requires six integrations.

B.3 Fresnel Magnetic Field

The electric field in the Fresnel zone due to an x-polarized aperture field was shown in Equation (8) to be

$$\vec{E}(\vec{r}) = \frac{jk_o e^{-jk_o r}}{2\pi r}(\hat{\theta}\cos\phi - \hat{\phi}\sin\phi)\int\int_{S'} E_x^a(\rho',\psi')e^{jk_o[\hat{r}\cdot\vec{\rho}' - \rho'^2/2r + (\hat{r}\cdot\vec{\rho}')^2/2r]}dS' \quad (30)$$

The corresponding magnetic field can be computed from the above by Ampere's Law for free space:

$$\vec{H}(\vec{r}) = -\frac{1}{j\omega\mu_o}\nabla\times\vec{E} \quad (31)$$

The two components of $\vec{H}$ in spherical coordinates are expressed by

$$-j\omega\mu_o H_\theta = -\frac{1}{r}\frac{\partial}{\partial r}(rE_\phi) \quad (32)$$

$$-j\omega\mu_o H_\phi = \frac{1}{r}\frac{\partial}{\partial r}(rE_\theta) \quad (33)$$

Using

$$\frac{\partial}{\partial r}[e^{-jk_o(r-\xi/2r)}] = -jk_o(1+\xi/2r^2)e^{-jk_o(r-\xi/2r)} \quad (34)$$

where $\xi = -\rho'^2 + (\hat{r}\cdot\vec{\rho}')^2$, the magnetic field in the Fresnel zone becomes

$$\vec{H}(\vec{r}) = \frac{jk_o e^{-jk_o r}}{2\pi\eta_o r}(\hat{\theta}\sin\phi + \hat{\phi}\cos\phi)\cdot \int\int_{S'}(1+\xi/2r^2)E_x^a(\rho',\psi')e^{jk_o[\hat{r}\cdot\vec{\rho}' - \rho'^2/2r + (\hat{r}\cdot\vec{\rho}')^2/2r]}dS' \quad (35)$$

Since $|\xi| \le 2\rho'^2 \le 2a^2$, where a is the aperture radius, then, for $a^2 \ll r^2$,

$$\vec{H}(\vec{r}) \approx \frac{\vec{r}\times\vec{E}}{\eta_o} \quad (36)$$

Thus, at distances greater than a few aperture radii, the electromagnetic field in the Fresnel zone behaves approximately as a spherical TEM wave.

Equation (36) was used for reducing Equation (24) to Equation (28) (see Equation (26)). When Equation (26) is used in Equation (24), a term proportional to

$$\vec{E}^a\times(\hat{r}\times\vec{E}^s)\cdot\hat{z} \quad (37)$$

results in the numerator. This term reduces to

$$[\hat{r}(\vec{E}^a \cdot \vec{E}^s) - \vec{E}^s(\vec{E}^a \cdot \hat{r})] \cdot \hat{z} = \hat{r} \cdot \hat{z}(\vec{E}^a \cdot \vec{E}^s) - \hat{z} \cdot \vec{E}^s(\vec{E}^a \cdot \hat{r}) \quad (38)$$

$$\approx \vec{E}^a \cdot \vec{E}^s \quad (39)$$

for $\hat{r} \cdot \hat{z} \approx 1$. This condition is satisfied at distances beyond a few aperture radii.

B.4 Reference

1. Ming-Kuei Hu, "Near-Zone Power Transmission Formulas", IRE National Convention Record, 1958, pp. 128-138.

UNCLASSIFIED

SECURITY CLASSIFICATION OF THIS PAGE

REPORT DOCUMENTATION PAGE

1a. REPORT SECURITY CLASSIFICATION Unclassified	1b. RESTRICTIVE MARKINGS
2a. SECURITY CLASSIFICATION AUTHORITY	3. DISTRIBUTION/AVAILABILITY OF REPORT Approved for public release; distribution is unlimited.
2b. DECLASSIFICATION/DOWNGRADING SCHEDULE	
4. PERFORMING ORGANIZATION REPORT NUMBER(S) TT-74	5. MONITORING ORGANIZATION REPORT NUMBER(S) ESD-TR-89-167
6a. NAME OF PERFORMING ORGANIZATION Lincoln Laboratory, MIT 6b. OFFICE SYMBOL *(If applicable)*	7a. NAME OF MONITORING ORGANIZATION Electronic Systems Division
6c. ADDRESS *(City, State, and Zip Code)* P.O. Box 73 Lexington, MA 02173-9108	7b. ADDRESS *(City, State, and Zip Code)* Hanscom AFB, MA 01731
8a. NAME OF FUNDING/SPONSORING ORGANIZATION Defense Advanced Research Projects Agency 8b. OFFICE SYMBOL *(If applicable)* DARPA/TTO	9. PROCUREMENT INSTRUMENT IDENTIFICATION NUMBER F19628-85-C-0002
8c. ADDRESS *(City, State, and Zip Code)* 1400 Wilson Boulevard Arlington, VA 22209	10. SOURCE OF FUNDING NUMBERS PROGRAM ELEMENT NO. 62702E; PROJECT NO. 741; TASK NO.; WORK UNIT ACCESSION NO AO3391

11. TITLE *(Include Security Classification)*
Flashlight Radar: A Three-Dimensional Imaging Radar

12. PERSONAL AUTHOR(S)
Dennis J. Blejer, Richard L. Ferranti, Richard M. Burnes, William W. Irving, Shawn M. Verbout

13a. TYPE OF REPORT	13b. TIME COVERED	14. DATE OF REPORT *(Year, Month, Day)*	15. PAGE COUNT
Project Report	FROM _____ TO _____	1989, August, 10	50

16. SUPPLEMENTARY NOTATION
None

17. COSATI CODES		
FIELD	GROUP	SUB-GROUP

18. SUBJECT TERMS *(Continue on reverse if necessary and identify by block number)*
three-dimensional imaging radar; focused-beam antenna scatterometer; polarimetric calibration; FM-CW radar; backscatter theory; range deconvolution; camouflage

19. ABSTRACT *(Continue on reverse if necessary and identify by block number)*

In support of several programs at Lincoln Laboratory, a small focused-beam polarimetric, millimeter-wave radar scatterometer (an instrument for measuring radar cross section) has been developed. An overview of the design of this "Flashlight Radar" is presented. Theoretical and empirical studies of antenna performance are discussed. The backscatter theory relating to the characteristics of the Flashlight Radar as a scatterometer is presented, and experimental RCS measurements are compared with theoretical predictions. The data processing steps (polarimetric calibration and compensation, signal processing, and image formation) are described. We show the results of two representative experiments using the Flashlight Radar. The first is a measurement of dihedral and trihedral reflectors with and without radar camouflage. The second is a raster scan of a truck tire, highlighting the radar's fine resolution and its ability to collect three-dimensional data.

20. DISTRIBUTION/AVAILABILITY OF ABSTRACT	21. ABSTRACT SECURITY CLASSIFICATION
☐ UNCLASSIFIED/UNLIMITED ☒ SAME AS RPT. ☐ DTIC USERS	Unclassified
22a. NAME OF RESPONSIBLE INDIVIDUAL Lt. Col. Hugh L. Southall, USAF	22b. TELEPHONE *(Include Area Code)* (617) 981-2330 — 22c. OFFICE SYMBOL ESD/TML

DD FORM 1473, 84 MAR — 83 APR edition may be used until exhausted. All other editions are obsolete.

UNCLASSIFIED

SECURITY CLASSIFICATION OF THIS PAGE